ACS OMEGA

Open Access

http://pubs.acs.org/journal/acsodf

Article

Bioorthogonal Diels–Alder Click Chemistry-Based Pretargeted PET Imaging Strategy for Monitoring Programmed Death-Ligand 1 Expression

Yong Huang, Zhongjing Li, Chengze Li, Zihan Zang, Qiong Wang, Size Huang, Qi Liu,* and Ying Liang*

Cite This: *ACS Omega* 2024, 9, 36969–36981

Read Online

ACCESS | Metrics & More | Article Recommendations | Supporting Information

ABSTRACT: The development of antibody tracers for positron emission tomography (PET) imaging enables real-time monitoring of tumor expression of programmed cell death ligand 1 (PD-L1) *in vivo*, aiming to facilitate the selection of immunotherapy responders. However, the slow pharmacokinetics of the antibodies in vivo limits their applications in PET imaging with commonly used radionuclides with short half-lives. In this study, we developed a pretargeted PET imaging strategy based on Diels–Alder (IEDDA) click chemistry to overcome these limitations. Atezolizumab and durvalumab, the most commonly used PD-L1 antibodies in cancer immunotherapy, were selected and compared in the development of the pretargeted PET imaging strategy. Fluorine-18-labeled derivatives of methyl tetrazine ([^{18}F]Tz, [^{18}F]PEG$_6$-Tz, and [^{18}F]PEG$_{12}$-Tz) were tested in biodistribution and PET imaging of A549-PDL1 xenografts (PD-L1 positive) pretargeted with the trans-cyclooctene (TCO)-functionalized atezolizumab/durvalumab. The biodistribution and imaging results indicated that atezolizumab-TCO/[^{18}F]PEG$_{12}$-Tz was more suitable for pretargeted PET imaging strategy, and the optimal interval time was 48 h after atezolizumab-TCO administration, where the atezolizumab-TCO/[^{18}F]PEG$_{12}$-Tz pretargeted approach clearly delineated the A549-PDL1 tumor with a tumor-to-muscle ratio of 5.33, while the ratios are 3.39 and 2.39 for durvalumab/[^{18}F]PEG$_{12}$-Tz and mock-pretargeting controls, respectively. In conclusion, a pretargeted ^{18}F-immuno-PET imaging technology was successfully established on atezolizumab. The high-contrast PET images of the A549-PDL1 tumor models demonstrate that the pretargeting strategy incorporating short-lived fluorine-18 is viable in identifying tumors with high PD-L1 expression, marking this strategy as a potential candidate for further clinical translation.

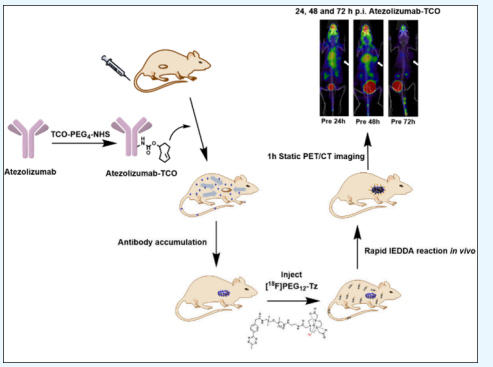

INTRODUCTION

Immune checkpoint proteins PD-L1 and PD-1 are critical targets for cancer immunotherapy. Tumor cells in the tumor microenvironment express PD-L1 through immunomodulatory mechanisms, allowing it to bind to PD-1 receptors on tumor-infiltrating lymphocytes. This interaction can lead to apoptosis of lymphocytes, thereby resisting their cytotoxic effects and ultimately enabling immune escape of the tumor.[1−3] Clinical studies have demonstrated that the expression of PD-L1 in tumor tissues is associated with the efficacy of anti-PD-1/PD-L1 immunotherapy.[4−7] Moreover, immunotherapy using monoclonal antibodies against PD-L1 has been found to yield substantial clinical benefits in patients whose tumors display positive PD-L1 expression.[8−10] Therefore, it is of vital importance to assess the *in vivo* expression of PD-L1 in tumor lesions. However, the existing methods for evaluating the expression status of PD-L1 rely on biopsy samples, which may not comprehensively represent the entire tumor tissue, including metastatic lesions. PET molecular imaging has demonstrated potential in noninvasively detecting cancer biomarkers in both primary and metastatic tumors, thereby enabling the screening of patients who might respond favorably to molecular targeted therapies.[11−13]

Recent reports have described PET targeting probes for PD-L1, including antibody-based probes,[14−18] peptide-based probes,[19−21] and small molecule inhibitors.[22−25] These probes have been utilized to assess the expression status of PD-L1 in patients with various types of solid tumors.[14,15,26,27] The key to achieving PET imaging is the selection of molecular probe ligands. Compared with peptides and small molecule inhibitors, antibodies with high specificity and affinity have always been the preferred choice for immune-PET molecular imaging research. Currently, relevant PD-L1 antibodies have been studied using radioisotope labeling in tumor models that

Received: February 2, 2024
Revised: July 5, 2024
Accepted: August 14, 2024
Published: August 21, 2024

express PD-L1, and their visualization has been conducted. However, the use of antibody macromolecules as tracers requires labeling with long half-life radioisotopes due to slow pharmacokinetics, which leads to excessive radiation doses to healthy organs.[28,29] Moreover, the long half-life of PET radioisotopes such as ^{89}Zr, ^{124}I, and ^{64}Cu presents challenges in terms of cost, complex preparation processes, and difficulties in acquisition, which hinders their clinical translation.[30−33]

The pretargeting strategy using a rapid bioorthogonal Diels−Alder reaction between trans-cyclooctene (TCO) and tetrazine (Tz) can alleviate the above complications.[34−40] In pretargeted imaging, a TCO-modified antibody is first injected and allowed to accumulate completely at the target site. Then, a radioligand is added that selectively binds to the TCO-modified antibody, while the excess radioligand is rapidly cleared due to its small molecular weight. In the past decade, Diels−Alder click chemistry between Tz and TCO in imaging studies of different antibodies has been reported by many investigators.[41−46]

In this study, three ^{18}F-labeled methyl tetrazines ([^{18}F]Tz, [^{18}F]PEG$_6$-Tz, and [^{18}F]PEG$_{12}$-Tz) were used for studies and comparisons of pretargeted PET imaging. Two PD-L1 antibodies (durvalumab and atezolizumab) were chosen for this study because of their broad clinical applications in cancer immunotherapy. Ultimately, the pretargeted PET imaging strategies (atezolizumab-TCO/[^{18}F]PEG$_{12}$-Tz) we discovered could evaluate the expression level of PD-L1, efficiently differentiate tumors from normal tissues, and generate relatively high contrast PET images.

EXPERIMENTAL PROCEDURES

Reagents and Instruments. All reagents used in the experiment were commercially purchased and used without additional purification unless specified otherwise. Humanized PD-L1 antibodies (durvalumab and atezolizumab) were purchased from AstraZeneca and Roche Diagnostics GmbH, respectively. TCO-PEG$_4$-NHS Ester was purchased from Xi'an ruixi Biological Technology Co., Ltd. NOTA-Tz, NOTA-PEG$_6$-Tz and NOTA-PEG$_{12}$-Tz were purchased from Nanchang Tanzhen Biotechnology Co., Ltd. These labeling precursors were obtained at >95% chemical purity and identified using mass spectrometry (Figures S1−S3). The HPLC system employed was an Agilent 1260 Infinity II (USA). The radiation value of the cell experiment and biological distribution experiment was measured using a γ-counter (Hidex, Turku, Finland). Small animal imaging was conducted using a Madiclab PSA146 PET/CT/FMT instrument (Madic, Shandong, China). Radioactivity was measured utilizing a Capintec CAPRAC-R dose calibrator (NJ, USA).

[^{18}F]Fluoride was produced from DONGCHENG AMS (Guangdong) PHARMACEUTICAL with a HM-20 medical cyclotron (Sumitomo, Kyoto, Japan) as an [^{18}O] enriched aqueous solution of [^{18}F]fluoride. Solid-phase extraction (SPE) cartridges such as Sep-Pak QMA Light and C18 Light cartridges were purchased from Waters (Milford, MA).

Preparation and Purification of Durvalumab-TCO or Atezolizumab-TCO. Commercially available humanized PD-L1 antibodies (durvalumab and atezolizumab) were first purified using an activated PD-10 desalting column. Subsequently, 9 μL of saturated K_2CO_3 solution was added to 300 μL of 50 mg/mL durvalumab or atezolizumab in PBS buffer solution to give a final mixture of pH = 8.5−9. Finally, 40 μL of a TCO-PEG$_4$-NHS Ester (25 mg/mL) DMSO solution was added to the antibody solution. The reaction mixture was reacted at room temperature with slight stirring for 40 min. During the reaction, the PD-10 desalting column was equilibrated in advance with 25 mL of PBS pH = 7.4. The equilibrated PD-10 desalting column was used for the purification of the final product. After purification, the product durvalumab-TCO or atezolizumab-TCO was stored for a short period of time in PBS at 4 °C. The protein concentration and chemical purity of durvalumab-TCO or atezolizumab-TCO were determined by a size exclusion chromatography HPLC column (300 Å, 3 μm, 7.8 × 300 mm^2, BioCore SEC) running with 1 mL/min PBS. The TCO-to-durvalumab/atezolizumab ratio was determined by electrospray ionization-quadrupole-TOF-MS (ESI-Q-TOF-MS), calculating the mass difference of nonconjugated durvalumab/atezolizumab to TCO-conjugated TCO-durvalumab/atezolizumab.

Radiosynthesis of [^{18}F]Tz, [^{18}F]PEG$_6$-Tz, and [^{18}F]-PEG$_{12}$-Tz. ^{18}F$^-$ was loaded on a QMA cartridge pretreated with 5 mL of 0.5 M NaOAc buffer (pH = 3.9) and 5 mL of water and then obtained by eluting the QMA cartridge with 0.3 mL of 0.5 M NaOAc buffer (pH = 3.9). ^{18}F$^-$ eluent (300 μL, 2−5 GBq), $AlCl_3$ (10 μL, 2 mM), 300 μL of DMSO, and 50 μL of NOTA-Tz, NOTA-PEG$_6$-Tz, or NOTA-PEG$_{12}$-Tz (4 mM) were mixed. Then the mixture was heated at 100 °C for 15 min to accomplish the radioactive chelation reaction. After the end of the reaction, the mixture was cooled in an ice bath and added to 9 mL of water. The mixture was loaded onto an activated C18 cartridge, pushed through, and washed with 30 mL of water sequentially, and the desired radiolabeled compound was eluted with 1.5 mL of ethanol and water in a ratio of 1:1 (v/v), which was finally obtained by passing a sterile filter membrane (0.2 μm). Radiochemical purity of [^{18}F]Tz, [^{18}F]PEG$_6$-Tz, or [^{18}F]PEG$_{12}$-Tz was confirmed by an analytical C18 Radio-HPLC column (100 Å, 5 μm, 250 × 10 mm^2, Phenomenex Luna) running a linear gradient starting from 75% A (0.1% TFA in water) and 25% B (0.1% TFA in acetonitrile) for 2 min and decreasing to 20% A at 15 min at 3 mL/min.

Partition Coefficient. [^{18}F]Tz, [^{18}F]PEG$_6$-Tz, or [^{18}F]-PEG$_{12}$-Tz (37 kBq) was added to a mixture consisting of 5.0 mL of phosphate buffered saline (PBS) with a pH of 7.4 and 5.0 mL of 1-octanol in a 15 mL centrifuge tube. After vigorous vortexing for 5 min, the mixture was subsequently centrifuged at 10,000 rpm for 5 min to create two distinct phases. Subsequently, 100 μL samples were extracted from each phase, and the radioactivity was quantified using a γ-counter. The partition coefficient was calculated as $\mathrm{Log}_{10}D$ = Log_{10}(counts in 1-octanol/counts in PBS) (n = 3).

In Vitro Ligation of [^{18}F]Tz with Durvalumab/Atezolizumab-TCO. We tested the reactivity of [^{18}F]Tz to durvalumab-TCO or atezolizumab-TCO at room temperature and in PBS (pH = 7). Briefly, the radiolabeled product [^{18}F]Tz (500 μL, 0.37 GBq) was mixed with durvalumab/atezolizumab-TCO (300 μg, ∼2 nmol) and reacted with slight shaking at room temperature for 1, 5, 10, 20, 30, and 40 min. After the end of the reaction, an equilibrated PD-10 desalting column was used for the purification of the final product ([^{18}F]Tz-TCO-durvalumab/atezolizumab). The free fluorine-18, unreacted radiolabeled tetrazine ([^{18}F]Tz) and [^{18}F]Tz-TCO-durvalumab/atezolizumab were determined with SEC-HPLC.

In Vitro Serum Stability. The radiolabeled [^{18}F]PEG$_{12}$-Tz and [^{18}F]Tz-TCO-atezolizumab were added into normal human serum (0.2 mL) and incubated for 1 h at 37 °C.

https://doi.org/10.1021/acsomega.4c01063
ACS Omega 2024, 9, 36969−36981

Plasma protein was precipitated with 0.4 mL of acetonitrile and centrifuged (10,000 rpm, 5 min). The radiochemical purities of [^{18}F]PEG$_{12}$-Tz and [^{18}F]Tz-TCO-atezolizumab in supernatants were assayed by analytical Radio-HPLC columns (Phenomenex Luna C18 (100 Å, 5 μm, 250 × 10 mm^2) and BioCore SEC (300 Å, 3 μm, 7.8 × 300 mm^2), respectively).

Cell Lines and Tumor Models. Stably PD-L1-transfected A549-PDL1 cells (acquired using lentiviral infection, provided by the research group of Professor Yang Zhi from the Peking University Cancer Hospital) and A549 cells (purchased from the Institute of Biochemistry and Cell Biology, Shanghai, China) were used for the cell-based experiments. A549-PDL1 cells and A549 cells were cultured in RPMI-1640 medium (Gibco, Carlsbad CA, USA), supplemented with 15% fetal bovine serum (Gibco) and antibiotics (100 mg/mL streptomycin and 100 mg/mL penicillin; Gibco) at 37 °C in a humidified incubator with 5% CO_2.

For biodistribution and micro-PET imaging studies of [^{18}F]Tz, [^{18}F]PEG$_6$-Tz, [^{18}F]PEG$_{12}$-Tz, or pretargeted imaging, male BALB/c nude mice (weight 13−18 g, age 4−6 weeks) were implanted subcutaneously with 5 × 10^6 A549-PDL1 cells and A549 cells (in 100 μL PBS) behind right armpit. Mice were housed in a thermostatic animal room at 37 °C and imaged or used for biodistribution studies when tumor xenografts reached 5−10 mm in diameter.

Cell Assay. *Western Blot Analysis.* To observe the differences in PD-L1 expression in tumor cells, we performed Western blot experiments on A549-PDL1 and A549 cancer cells. Detailed procedures are described in the Supporting Information.

In Vitro Pretargeting Specificity. The feasibility of specific pretargeting of A549-PDL1 cells (PD-L1 expressing cancer cells) were tested using two commonly used PD-L1 monoclonal antibodies (durvalumab and atezolizumab). Briefly, the live cells were divided into groups of four. In one set of dishes, cells were preincubated with durvalumab/atezolizumab-TCO (100 μg) for 60 min at 37 °C, and dishes then were washed twice with cold PBS (pH = 7.4). Thereafter, [^{18}F]Tz (74 kBq) was added to the cells. After incubation for 60 min at 37 °C, the medium was removed, and then the cells were washed twice with cold PBS (pH = 7.4). The adherent cells were then lysed with 1 N NaOH at 37 °C for 5 min. The lysates were collected and measured with a γ-counter. The result was expressed as % ID/10^6 cells. The following two block experiments were also performed. In one set of dishes, cells were pretreated with a 50-fold molar excess of parental anti-PDL1 durvalumab/atezolizumab to prevent durvalumab/atezolizumab-TCO binding. In another set, 50 μg of unlabeled tetrazine (NOTA-Tz) was added to compete with the specific binding of [^{18}F]Tz. Other manipulations were as described above. To the fourth set, [^{18}F]Tz (74 kBq) was added directly to the cells without the addition of durvalumab/atezolizumab-TCO and the cells were incubated for 1 h.

Cellular Uptake and Internalization of [^{18}F]Tz-TCO-Durvalumab/Atezolizumab. A549-PDL1 cells were incubated with the radiolabeled compound for 30, 60, 120, and 180 min at 37 °C, and uptake was terminated by removing the medium from the cells and washing twice with 1 mL of ice-cold PBS. Subsequently, cells were incubated with 1 mL of glycine HCl (1 mol/L, pH 2.2) for 10 min at 37 °C to remove the surface-bound activity. Next, the cells were washed with 2 mL of ice-cold PBS and lysed with 1 mL of lysis buffer to determine the internalized fraction. The combined washes and lysate were measured to determine the cellular uptake value. Each experiment was performed three times, with three replicates for each independent experiment.

Saturation Binding Experiments. A concentration gradient of in vitro ligated purified probe of [^{18}F]Tz-TCO-durvalumab/atezolizumab, 0.08−10 nM, was added to wells and incubated with A549-PDL1 cells (2 × 10^5 cells/well) at 37 °C for 1 h. Nonspecific binding was performed by adding an excess of unlabeled durvalumab/atezolizumab (100-fold) to the wells 1 h prior to incubation with ligated [^{18}F]Tz-TCO-durvalumab/atezolizumab. Each condition was conducted three times for saturation binding experiments. Other manipulations were as described above. A nonlinear regression analysis with one site-specific binding equation was used to determine K_d using GraphPad Prism 9.5.

Micro-PET/CT Imaging and Immunohistochemical Staining. In order to screen the optimal tetrazine radioligand for pretargeted PET imaging, dynamic micro-PET imaging of 1 h with [^{18}F]Tz, [^{18}F]PEG$_6$-Tz, and [^{18}F]PEG$_{12}$-Tz was first performed in normal male athymic nude mice as a control group, and their pharmacokinetic profiles were investigated. For pretargeted PET imaging, male athymic nude mice bearing subcutaneous A549-PDL1 and A549 (right shoulder) xenografts were administered 300 μg of atezolizumab-TCO via intravenous tail vein injection. After 48 h cumulative interval, the A549-PDL1 model mice were then injected with [^{18}F]Tz, [^{18}F]PEG$_6$-Tz, and [^{18}F]PEG$_{12}$-Tz (3.7 MBq) also via intravenous tail vein injection. In addition, two additional cumulative intervals of 24 and 72 h were also conducted to explore the optimal time interval. For the control and blocking experiments, the A549-PDL1 tumor-bearing mice were injected with [^{18}F]PEG$_{12}$-Tz alone and co-injected with atezolizumab (2.5 mg/mouse). For direct PET imaging of [^{18}F]Tz-TCO-atezolizumab, male mice bearing subcutaneous A549-PDL1 xenografts were intravenously injected with [^{18}F]Tz-TCO-atezolizumab (7.4 MBq/mouse).

Micro-PET imaging studies were conducted in nude mice using a Madiclab PSA146 PET/CT/FMT instrument (Linyi, China). All animals were sedated with isoflurane anesthesia (2−3%, 1 L/min oxygen) and were then placed on a heating pad in order to maintain body temperature throughout the procedure. The raw data from PET/CT imaging of small animals were reconstructed using the 3D ordered subset expectation maximum (OSEM) algorithm to obtain whole-body PET images of mice, while the percentage of injected dose per gram of tissue (% ID/g) was used for quantitative analysis of tumor target areas. For data analysis, the regions of interest (ROIs) were manually drawn over the tumor and major organs on decay-corrected whole-body coronal images using PMOD software (version 4.3, PMOD Technologies Ltd., Zurich, Switzerland).

Immunohistochemistry (IHC) staining was performed on 3 μm thick sectioned tissue samples of the A549-PDL1 and A549 tumors. Detailed procedures are described in the Supporting Information.

Biodistribution. *Biodistribution of [^{18}F]Tz, [^{18}F]PEG$_6$-Tz, and [^{18}F]PEG$_{12}$-Tz.* Nude mice (female, weight 12−16 g) were purchased from Guangdong GemPharmatech Co., Ltd. Approximately 1.85 MBq of [^{18}F]Tz, [^{18}F]PEG$_6$-Tz, and [^{18}F]PEG$_{12}$-Tz was administered via tail vein injection in conscious animals. Three mice per group were euthanized at 60 min time point, organs were removed and weighed, and radioactivity was counted using a γ-counter. The radioactivity

https://doi.org/10.1021/acsomega.4c01063
ACS Omega 2024, 9, 36969−36981

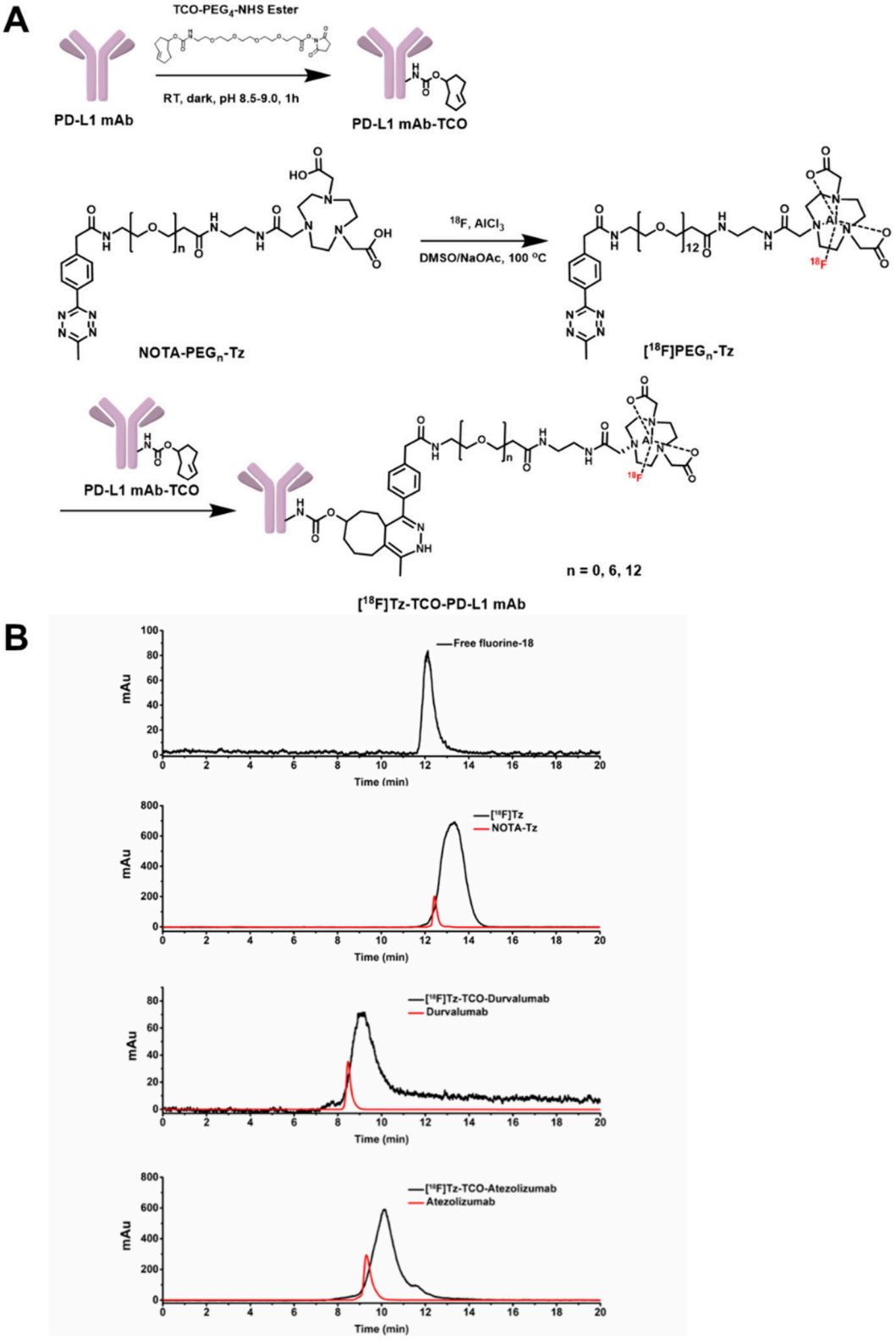

Figure 1. (A) TCO modification of PD-L1 mAb-TCO, radionuclide labeling of NOTA-PEG*n*-Tz, and Diels−Alder click reaction between PD-L1 mAb-TCO and [^{18}F]PEG*n*-Tz in vitro. (B) Reaction between free fluorine-18, unreacted radiolabeled tetrazine, and PD-L1 mAb-TCO identified by radio-SEC-HPLC (black line: radioactive profile; red line: UV profile).

in each organ was normalized as the percentage of injected dose per gram of tissue (% ID/g).

In Vivo Pretargeting Specificity. Nude mice bearing A549-PDL1 and A549 xenograft tumors were injected via the tail vein with durvalumab-TCO or atezolizumab-TCO (300 μg in 150 μL of PBS). After 24, 48, or 72 h, the mice were injected with [^{18}F]PEG$_{12}$-Tz (1.85 MBq). Other manipulations were as described above. The control experiments were also performed

https://doi.org/10.1021/acsomega.4c01063
ACS Omega 2024, 9, 36969−36981

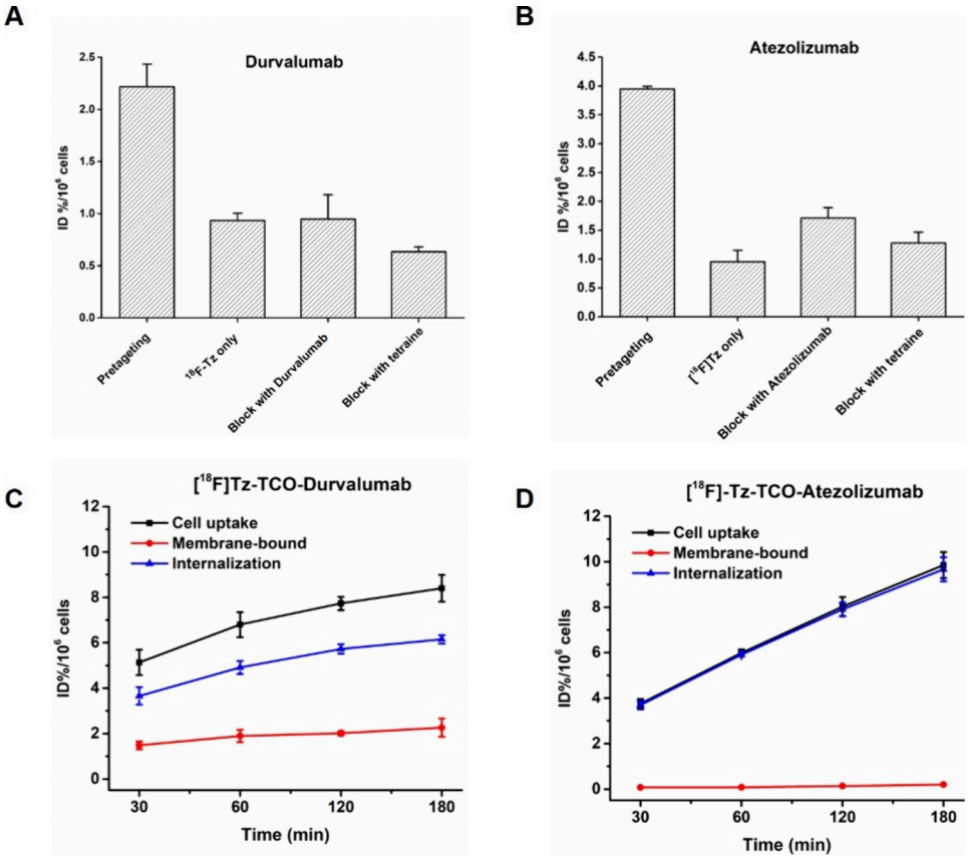

Figure 2. Binding of [^{18}F]Tz to A549-PDL1 cells preincubated with durvalumab-TCO (A) and atezolizumab-TCO (B) for 1 h before addition of [^{18}F]Tz (first bar in graph), for [^{18}F]Tz added directly to cells (second bar), for cells co-incubated with excess unmodified PD-L1 mAb and PD-L1 mAb-TCO for 60 min followed by addition of [^{18}F]Tz (third bar), and for cells preincubated with PD-L1 mAb-TCO followed by addition of excess unlabeled tetrazine and [^{18}F]Tz (fourth bar). Cellular uptake and internalization of [^{18}F]Tz-TCO-durvalumab (C) and [^{18}F]Tz-TCO-atezolizumab (D) in A549-PDL1 cells.

on mice bearing A549-PDL1. Briefly, [^{18}F]PEG$_{12}$-Tz (1.85 MBq) was injected directly into the mice without the addition of atezolizumab-TCO, and mice were euthanized after 1 h. For blocking experiments, mice were co-injected with a 50-fold molar excess of atezolizumab and 50 μg of unlabeled tetrazine (NOTA-PEG$_{12}$-Tz) to prevent atezolizumab-TCO and [^{18}F]-PEG$_{12}$-Tz binding, respectively.

Dosimetry. Internal radiation dose was estimated based on micro-PET/CT imaging of atezolizumab-TCO/[^{18}F]PEG$_{12}$-Tz pretargeting 48 h and [^{18}F]Tz-TCO-atezolizumab for in vivo injected nude male mice bearing A549-PDL1 tumor. The radiation dose estimates were calculated for human organs based on an extrapolation of the animal data to humans using the OLINDA (v.1.0 (2003)/EXM software.

Statistical Analysis. Quantitative data were reported as mean ± standard deviation (SD), and statistical differences between groups were assessed using Student's *t* test conducted with GraphPad Prism 9.5 software. A *P*-value of less than 0.05 was considered statistically significant.

RESULTS

Chemical and Radiochemical Results. TCO-modified durvalumab/atezolizumab was successfully prepared via reaction of the antibody with approximately 20-fold equivalent of NHS-PEG$_4$-TCO at room temperature for 60 min. The antibody protein recovery rate was 83.3 ± 5.0%, and the HPLC purification of the conjugate provided purity of >95%. The mass spectrum of the purified durvalumab-TCO (found 152.6, 152.2, 153.4, 153.8, 151.8, 153.0 kDa) and atezolizumab-TCO (found 149.2, 149.6, 150.0, 150.4, 148.4, 148.8 kDa) are shown in Figures S4 and S5. ESI-Q-TOF-MS confirmed the presence of an average of 12 TCO molecules per durvalumab molecule and 8 TCO molecules per atezolizumab molecule.

[^{18}F]Tz, [^{18}F]PEG$_6$-Tz, and [^{18}F]PEG$_{12}$-Tz were radionuclide labeled by complexing Al^{18}F with a NOTA chelator and successfully produced by one-step manual labeling (Figure 1A). The non-decay-corrected radiochemical yield of [^{18}F]Tz, [^{18}F]PEG$_6$-Tz, and [^{18}F]PEG$_{12}$-Tz was 15.1% ± 2.0% (n = 23), 12.3% ± 3.0% (n = 11), and 11.1% ± 3.0% (n = 27), respectively. The specific activities of [^{18}F]Tz, [^{18}F]PEG$_6$-Tz, and [^{18}F]PEG$_{12}$-Tz based on radioactivity measurements were determined to be 4.1, 2.6, and 3.4 GBq/μmol, respectively. The radiochemical purity of [^{18}F]Tz, [^{18}F]PEG$_6$-Tz, and [^{18}F]PEG$_{12}$-Tz was >98% with retention times of 7.68, 8.95, and 9.03 min (Figure S6), respectively. The entire radionuclide labeling time was approximately 20 min, including radionuclide labeling and product purification procedures. The log D values of [^{18}F]Tz, [^{18}F]PEG$_6$-Tz, and [^{18}F]PEG$_{12}$-Tz were calculated to be −2.09 ± 0.02, −2.42 ± 0.06 and −3.01 ± 0.08, indicating that as the number of PEG groups increases, the hydrophilicity of the compound becomes increasingly stronger.

By calculating the radioactivity ligation yield of durvalumab-TCO with [^{18}F]Tz for different reaction times, we found that

https://doi.org/10.1021/acsomega.4c01063
ACS Omega 2024, 9, 36969−36981

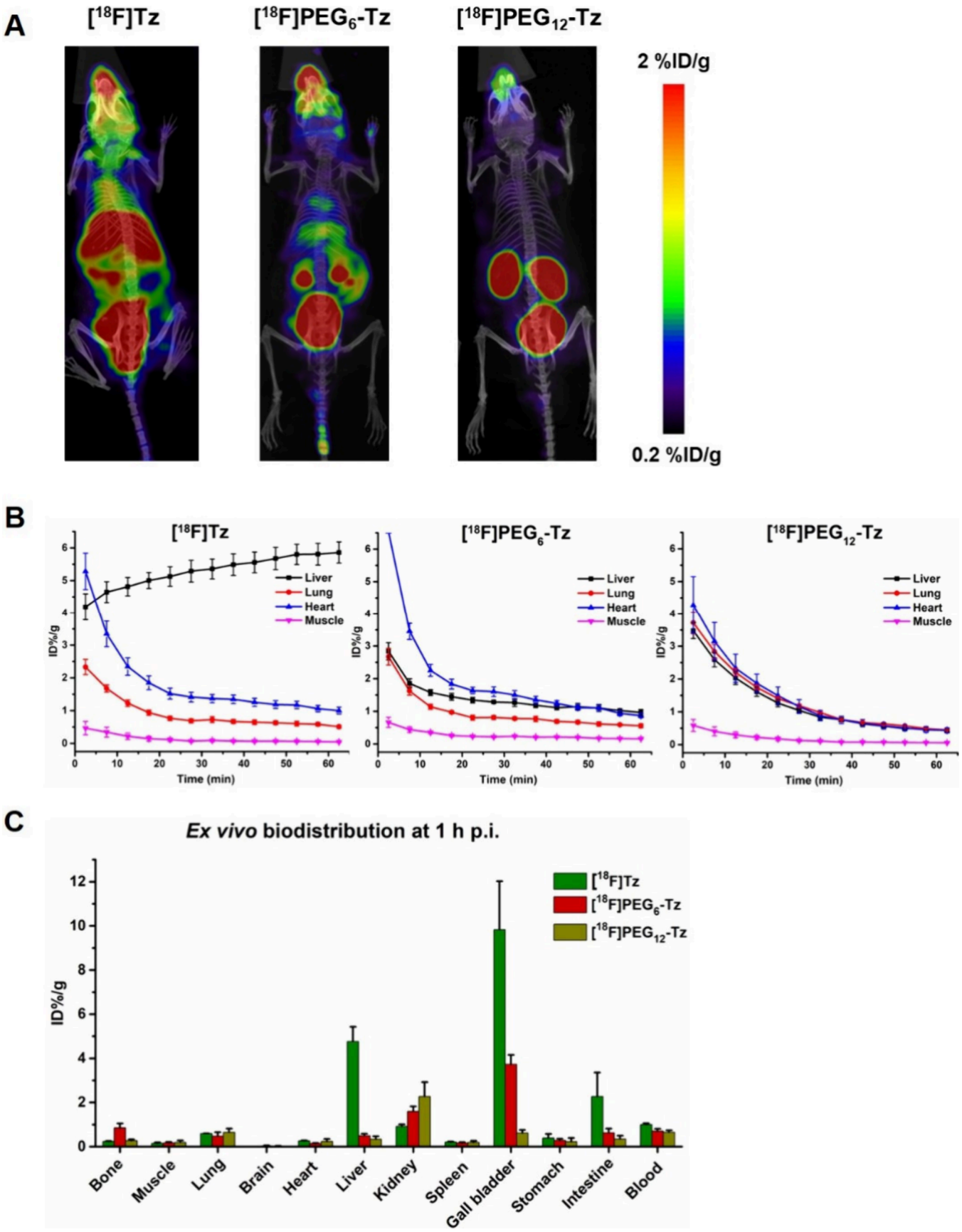

Figure 3. Micro-PET/CT imaging (A) and time−activity curves of organs (B) of [^{18}F]Tz, [^{18}F]PEG$_6$-Tz, and [^{18}F]PEG$_{12}$-Tz in normal mice. (C) *Ex vivo* biodistribution of [^{18}F]Tz, [^{18}F]PEG$_6$-Tz, and [^{18}F]PEG$_{12}$-Tz at 1 h after injection (n = 3).

https://doi.org/10.1021/acsomega.4c01063
ACS Omega 2024, 9, 36969−36981

Table 1. Biodistribution in Live Mice Bearing Subcutaneous A549-PDL1 Xenografts Preinjected with Atezolizumab/Durvalumab-TCO (300 μg in PBS) Followed 24, 48, and 72 h Later by [^{18}F]PEG$_{12}$-Tz[a]

	atezolizumab pretargeted			durvalumab pretargeted		
organ	24 h	48 h	72 h	24 h	48 h	72 h
bone	0.38 ± 0.07	0.28 ± 0.02	0.38 ± 0.03	1.16 ± 0.27	0.98 ± 0.26	0.53 ± 0.04
muscle	0.26 ± 0.04	0.31 ± 0.08	0.29 ± 0.06	0.72 ± 0.10	0.56 ± 0.20	0.43 ± 0.06
lung	1.78 ± 0.34	1.65 ± 0.11	0.92 ± 0.06	7.06 ± 1.90	3.19 ± 1.02	2.01 ± 0.06
brain	0.06 ± 0.01	0.05 ± 0.01	0.05 ± 0.01	0.29 ± 0.07	0.16 ± 0.04	0.14 ± 0.01
heart	0.93 ± 0.05	1.02 ± 0.14	0.74 ± 0.28	2.66 ± 0.49	1.57 ± 0.27	1.40 ± 0.28
liver	0.87 ± 0.08	0.96 ± 0.18	0.71 ± 0.16	1.93 ± 0.59	1.19 ± 0.23	1.01 ± 0.16
kidney	2.04 ± 0.09	2.82 ± 0.52	2.22 ± 0.37	3.12 ± 0.31	2.68 ± 0.46	2.27 ± 0.37
spleen	0.71 ± 0.04	0.71 ± 0.12	0.81 ± 0.13	1.27 ± 0.22	0.48 ± 0.34	0.62 ± 0.13
gall bladder	0.94 ± 0.11	0.94 ± 0.24	0.63 ± 0.21	1.29 ± 0.08	1.11 ± 0.35	0.99 ± 0.22
stomach	0.40 ± 0.16	0.37 ± 0.06	0.32 ± 0.11	0.50 ± 0.06	0.33 ± 0.09	0.75 ± 0.28
intestine	0.51 ± 0.12	0.62 ± 0.22	0.55 ± 0.15	0.54 ± 0.14	0.40 ± 0.07	0.51 ± 0.15
blood	1.72 ± 0.09	1.86 ± 0.15	1.48 ± 0.50	8.80 ± 0.50	6.08 ± 1.82	5.29 ± 0.50
A549-PDL1 tumor	1.16 ± 0.06	1.65 ± 0.29	0.90 ± 0.23	2.52 ± 0.16	1.91 ± 0.38	1.60 ± 0.23
tumor/muscle	4.40 ± 0.76	5.33 ± 0.68	3.13 ± 0.10	3.51 ± 0.75	3.39 ± 0.46	3.68 ± 0.98
tumor/blood	0.67 ± 0.01	0.89 ± 0.11	0.61 ± 0.03	0.29 ± 0.04	0.31 ± 0.07	0.30 ± 0.02

[a]The animals were euthanized, and tissues of interest were harvested 1 h after [^{18}F]PEG$_{12}$-Tz injection. Values are expressed as mean ± SD (% ID/g) (n = 3).

10 min was the optimal reaction time for obtaining the most radioactive product (Table S1). Durvalumab-TCO was indirectly radiolabeled with [^{18}F]Tz in 39.58 ± 1.7% (n = 3) radiochemical yield with a specific activity of 0.37 MBq/μg (55.5 MBq/nmol) (Figure 1A). The radiochemical purity of [^{18}F]Tz-TCO-durvalumab and [^{18}F]Tz-TCO-atezolizumab was >95% with retention times of 8.99 and 10.17 min, respectively, when analyzed using radio-HPLC (Figure 1B). The stability of [^{18}F]PEG$_{12}$-Tz and [^{18}F]Tz-TCO-atezolizumab was assayed in vitro by incubation in normal human serum (0.2 mL) for 1 h at 37 °C and subsequent HPLC analysis. The [^{18}F]PEG$_{12}$-Tz and [^{18}F]Tz-TCO-atezolizumab remained relatively stable in normal human serum after 1 h incubation (Figure S7).

Western Blotting, In Vitro Binding Specificity, Cellular Uptake, and Internalization. The results of Western blotting showed that A549-PDL1 cell lines overexpressed PD-L1 and the A549 cell lines expressed relatively low levels of PD-L1 protein (Figure S8).

In vitro binding of [^{18}F]Tz to durvalumab/atezolizumab-TCO pretreated A549-PDL1 (PD-L1 positive expressed) cells exceeded nonspecific uptake by untreated cells by 2.28- and 4.14-fold (Figure 2A,B). In addition, there was a highly significant reduction of [^{18}F]Tz binding to A549-PDL1 cells when durvalumab/atezolizumab-TCO binding was prevented by presaturation of receptors using unmodified anti-PD-L1 antibody or under competition with a large excess of nonlabeled tetrazine (Figure 2A,B). These data demonstrate that [^{18}F]Tz binding depends on the interaction of durvalumab/atezolizumab-TCO with PD-L1 and on the interaction of tetrazine with TCO, which confirms the feasibility of in vitro pretargeting.

Cellular uptake experiments of [^{18}F]Tz-TCO-durvalumab and [^{18}F]Tz-TCO-atezolizumab were performed to evaluate the ability of the two antibodies to bind to PD-L1. Shown in Figure 2C,D, the accumulation of [^{18}F]Tz-TCO-durvalumab, [^{18}F]Tz-TCO-atezolizumab in A549-PDL1 cells quickly reached 5.13 and 3.76 % ID/10^6 cells at 30 min, respectively. As the time was extended to 180 min, the uptake of both compounds increased. Compared to [^{18}F]Tz-TCO-durvalumab, the cellular uptake of [^{18}F]Tz-TCO-atezolizumab has a greater increase over time. The uptake of [^{18}F]Tz-TCO-durvalumab and [^{18}F]Tz-TCO-atezolizumab increased to 8.40 and 9.85 % ID/10^6 cells at 180 min, respectively. The internalization test showed that durvalumab and atezolizumab are endocytosed antibodies, but there is no significant correlation between the rate of internalization and the incubation time. The significant difference lies in the fact that [^{18}F]Tz-TCO-atezolizumab shows a very high internalization rate of 98.1% in A549-PDL1 cells, which is much higher than the internalization rate of 73.2% for [^{18}F]Tz-TCO-durvalumab at 180 min. In saturation binding assays, nonspecific (NS) binding of [^{18}F]Tz-TCO-durvalumab and [^{18}F]Tz-TCO-atezolizumab remained relatively constant (Figure S9). The specific binding (SB) curve showed a typical sigmoidal shape, with binding affinities of K_d = 2.39 and 1.38 nM, respectively.

Micro-PET/CT Imaging, Biodistribution, and Immunohistochemistry Analysis. We first performed micro-PET/CT imaging and biodistribution studies with [^{18}F]Tz, [^{18}F]PEG$_6$-Tz, and [^{18}F]PEG$_{12}$-Tz to investigate their pharmacokinetic profile. Dynamic micro-PET images and time−activity curves (Figure 3A,B) showed that [^{18}F]Tz was characterized by rapid tissue distribution and subsequent main clearance via the hepatobiliary system with a small amount cleared through the urinary system. [^{18}F]Tz quickly entered the liver and showed a large amount of retention at 5.86 ± 0.43% injected dose per gram (% ID/g) at 60 min after injection. In contrast, both [^{18}F]PEG$_6$-Tz and [^{18}F]PEG$_{12}$-Tz exhibited rapid urinary system elimination characteristics. The radioactive ligands can quickly enter the bloodstream, pass through the glomeruli, and ultimately be excreted from the bladder. The data show accumulation and retention of the [^{18}F]PEG$_6$-Tz and [^{18}F]PEG$_{12}$-Tz in the liver at 0.72 ± 0.12 and 0.43 ± 0.05 % ID/g at 60 min after injection. *Ex vivo* biodistribution data of [^{18}F]Tz, [^{18}F]PEG$_6$-Tz, and [^{18}F]-PEG$_{12}$-Tz were obtained in normal mice by injecting the tetrazine radioactive ligands via the tail vein (Figure 3C). The accumulation of [^{18}F]Tz, [^{18}F]PEG$_6$-Tz, and [^{18}F]PEG$_{12}$-Tz in liver after 60 min of injection was 4.76 ± 0.67, 0.50 ± 0.08, and

https://doi.org/10.1021/acsomega.4c01063
ACS Omega 2024, 9, 36969−36981

0.34 ± 0.13 % ID/g, respectively. These phenomena are consistent with PET imaging studies. The results of the above experiment suggest that the stronger the hydrophilicity of the tetrazine radioligand, the less likely it is to undergo hepatic and biliary metabolism. It is worth noting that although [^{18}F]PEG$_6$-Tz showed low uptake in several major organs, it has a very high radioactive uptake value of 3.73 ± 0.42 % ID/g in the gallbladder, which may interfere with the delineation of tumors in the liver and gallbladder area. Compared to [^{18}F]Tz and [^{18}F]PEG$_6$-Tz, [^{18}F]PEG$_{12}$-Tz exhibited faster in vivo clearance capacity and relatively lower radioactive uptake in various nontarget organs (<0.65 % ID/g), except for that in the excretion organ (kidneys) with moderate uptake (2.27 ± 0.65 % ID/g). Therefore, in the subsequent pretargeted research, we used [^{18}F]PEG$_{12}$-Tz as the main tetrazine radioactive ligand.

Three accumulation intervals of 24, 48, and 72 h were evaluated in A549-PDL1 tumor-bearing nude mice to validate the optimal interval between the injection of the durvalumab/atezolizumab-TCO and the administration of [^{18}F]PEG$_{12}$-Tz (Table 1). Data at an interval of 24 h after injection of durvalumab-TCO showed the highest tumor uptake (2.52 ± 0.16 % ID/g at 1 h [^{18}F]PEG$_{12}$-Tz p.i.) compared to 48 h (1.91 ± 0.38 % ID/g) and 72 h (1.60 ± 0.23 % ID/g), whereas the other tissues, including blood and lung, exhibited high uptake (8.80 ± 0.50 and 7.06 ± 1.90 % ID/g, respectively) and resulted in a low tumor-to-blood ratio of 0.29. The high accumulation of durvalumab in the blood and slow clearance creates a high background noise in the body, leading to a relatively low tumor-to-muscle ratio of only 3.51. In contrast, the uptake of A549-PDL1 tumor reached its highest value (1.65 ± 0.15 % ID/g) at 48 h after the injection of atezolizumab-TCO. Afterward, the uptake in the tumor gradually decreases. Moderate levels of radioactive uptake were observed in the blood and lungs (1.86 ± 0.15 and 1.65 ± 0.11 % ID/g, respectively). In addition, other organs such as the liver, muscles, bones, and intestines exhibited relatively low levels of uptake (<0.96 % ID/g) resulting in a tumor-to-muscle ratio of 5.33, which is higher than that at 24 h (4.40) and 72 h (3.13). Comparing the pretargeted biodistribution characteristics of durvalumab-TCO and atezolizumab-TCO, we found that atezolizumab-TCO is more suitable for pretargeted research for monitoring PD-L1 expression *in vivo*.

Pretargeted atezolizumab-TCO/[^{18}F]PEG$_{12}$-Tz imaging is shown in Figure 4A,B, which were consistent with the results of biodistribution. The imaging data obtained after injection of atezolizumab-TCO indicated that tumor uptake at a 48 h interval (0.94 ± 0.16 % ID/g at 1 h postinjection of [^{18}F]PEG$_{12}$-Tz) is higher compared to that at intervals of 24 h (0.79 ± 0.06 % ID/g) and 72 h (0.41 ± 0.04 % ID/g), as well as significantly higher than tumor uptake with only [^{18}F]PEG$_{12}$-Tz injection (0.28 ± 0.10 % ID/g). The experimental results further confirm that 48 h is a promising interval between the administration of atezolizumab-TCO and the subsequent injection of [^{18}F]PEG$_{12}$-Tz.

Pretargeted PET imaging and biodistribution using subcutaneously implanted A549 tumors with low PD-L1 expression demonstrated a significant reduction in radioactivity accumulation in the tumor, which was indistinguishable from the surrounding tissue (Figure 5A,C and Figure 6). Statistical analysis revealed that the radiotracer accumulation in A549 tumors was significantly lower than that in A549-PDL1 tumors in pretargeted interval of 48 h (P < 0.05). In two additional

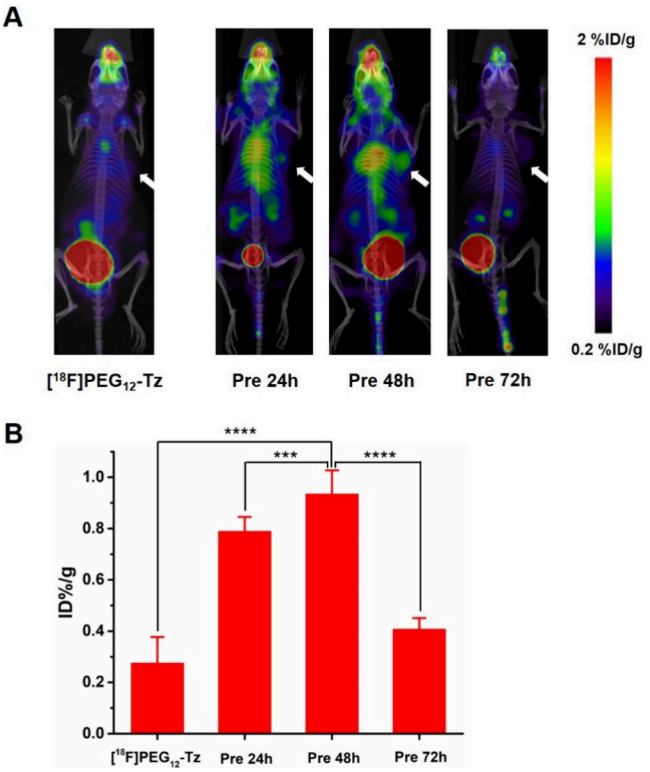

Figure 4. (A) Micro-PET images of [^{18}F]PEG$_{12}$-Tz directly injected and preinjected with atezolizumab-TCO (300 μg in PBS) followed 24, 48, and 72 h later by [^{18}F]PEG$_{12}$-Tz; white arrow indicates tumor area. (B) Uptake value of A549-PDL1 tumor at 1 h postinjection of [^{18}F]PEG$_{12}$-Tz (***P < 0.05; ****P < 0.0001).

blocking groups, mice bearing A549-PDL1 xenografts were either pretreated with unmodified atezolizumab followed by the same dose of the tetrazine radioligand or co-injected with a nonlabeled tetrazine. Both groups also exhibited a significant reduction in radioactivity accumulation in the A549-PDL1 tumor (P < 0.05). By calculation, the molar ratios of TCO to Tz used in the pretargeted PET imaging and Tz blocking conditions were 29.6 and 0.37, respectively. The results of immunohistochemistry sections of A549-PDL1 and A549 tumors are shown in Figure 5E. The A549-PDL1 tumor showed a high expression of PD-L1 in the cytoplasm and on the membranes (claybank), and the A549 tumor showed low PD-L1 expression, which was consistent with the results of PET imaging.

A comparison of pretargeted atezolizumab-TCO/[^{18}F]-PEG$_{12}$-Tz imaging and direct PET imaging at 8 h postinjection of [^{18}F]Tz-TCO-atezolizumab was performed using PD-L1-positive A549-PDL1 xenografts (Figure 5B,D). PET images of [^{18}F]Tz-TCO-atezolizumab at 8 h postinjection showed tumor-to-muscle uptake ratios comparable to atezolizumab pretargeting (19.9 vs 21.6), whereas tumor-to-liver uptake ratios were much lower than atezolizumab pretargeting (0.19 vs 1.49).

We further confirmed the rationality of [^{18}F]PEG$_{12}$-Tz as a pretargeted radioligand. Pretargeted PET imaging was performed using a 48 h interval of atezolizumab-TCO/[^{18}F]Tz and atezolizumab-TCO/[^{18}F]PEG$_6$-Tz in A549-PDL1 tumors (Figure S10). The imaging results indicated that in comparison to atezolizumab-TCO/[^{18}F]Tz and atezolizumab-TCO/[^{18}F]PEG$_6$-Tz, the pretargeted imaging

https://doi.org/10.1021/acsomega.4c01063
ACS Omega 2024, 9, 36969−36981

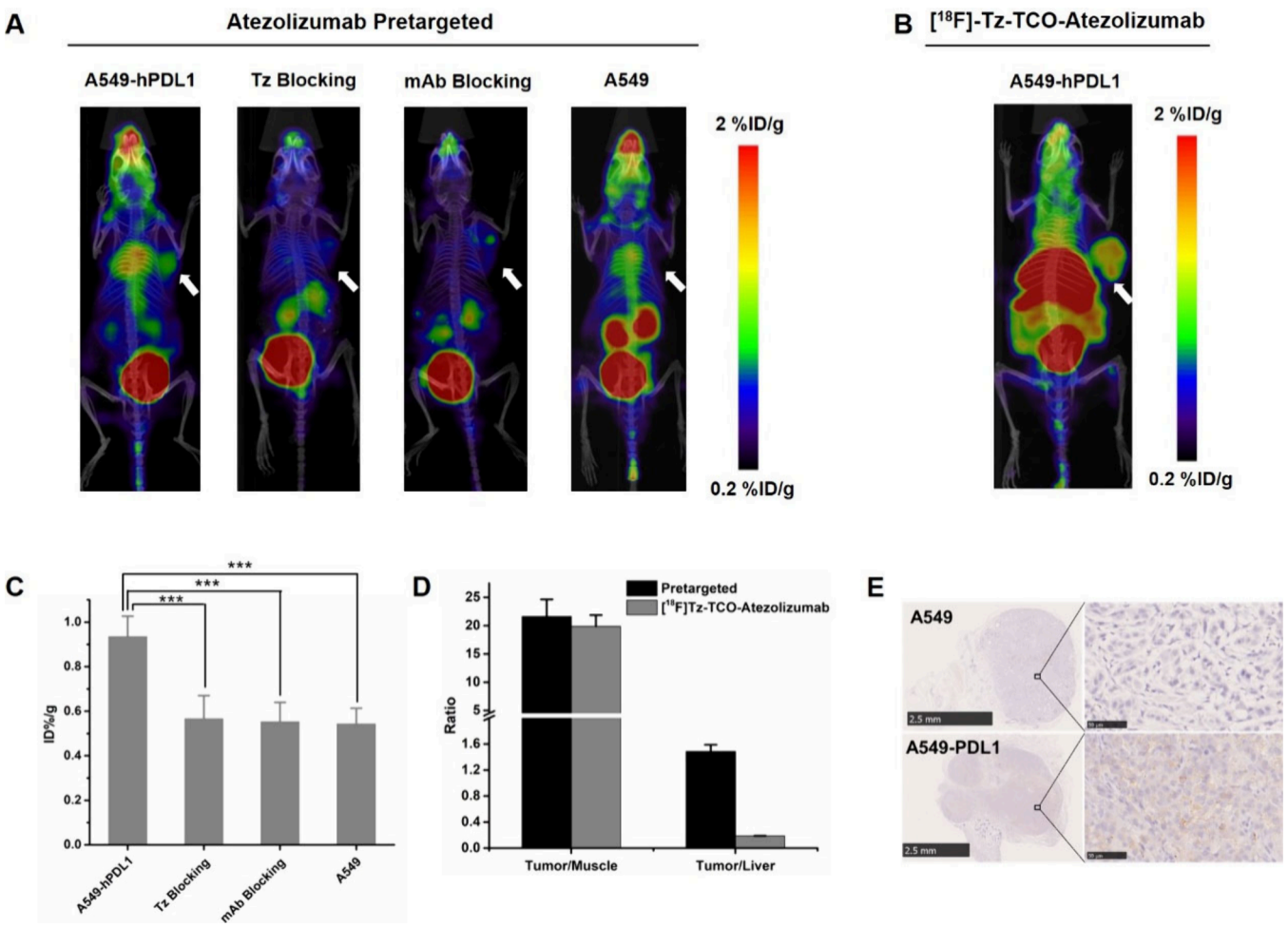

Figure 5. (A) Pretargeted atezolizumab-TCO/[^{18}F]PEG$_{12}$-Tz images in A549-PDL1 and A549 tumor-bearing nude mice; the tumors are indicated by white arrows. (B) Static PET images at 8 h postinjection of [^{18}F]Tz-TCO-atezolizumab in male mice bearing subcutaneous A549-PDL1 xenografts. (C) Uptake or block value of A549-PDL1 and A549 tumor at 1 h postinjection of [^{18}F]PEG$_{12}$-Tz (***$P < 0.05$). (D) Ratios of A549-PDL1 tumor/muscle and tumor/liver. (E) Immunohistochemical analysis for PD-L1 expression demonstrating high immunoreactivity (claybank) in A549-PDL1 and low immunoreactivity in A549 tumor.

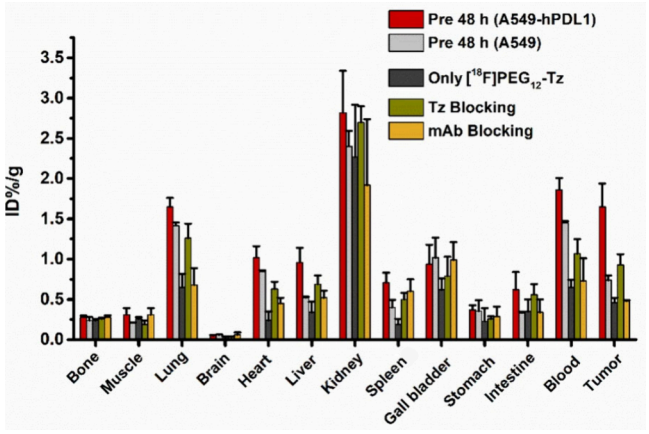

Figure 6. (A) Pretargeted atezolizumab-TCO/[^{18}F]PEG$_{12}$-Tz biodistribution in A549-PDL1 and A549 tumor-bearing nude mice.

approach utilizing atezolizumab-TCO/[^{18}F]PEG$_{12}$-Tz exhibited superior efficacy in evaluating the PD-L1 expression levels and yielded PET images with relatively higher contrast.

Dosimetry. We assessed the radiation dose associated with this pretargeting strategy using the PET imaging data for the atezolizumab-TCO/[^{18}F]PEG$_{12}$-Tz pretargeting methodology and the direct PET imaging data at 1, 2, 4, 6, and 8 h postinjection of [^{18}F]Tz-TCO-atezolizumab (Tables S2 and S3). As expected, the pretargeting strategy resulted in a significant reduction in radiation exposure, compared with the [^{18}F]Tz-TCO-atezolizumab radioimmunoconjugate, lowering the total effective dose by over 7.5-fold (Table S4). The effective internal radiation dose of the atezolizumab-TCO/[^{18}F]PEG$_{12}$-Tz pretargeting methodology was calculated to be 1.15×10^{-3} μSv/MBq for men, which was lower than the FDA limit for research subjects in a single study.

DISCUSSION

In order to match the slow pharmacokinetics of antibodies, immunoPET studies prefer long-lived radionuclides. However, the prolonged retention of long half-life nuclide-labeled antibody imaging agents in the body increases the radioactive dose to nontarget tissues. Meanwhile, the slow pharmacokinetics and slow tumor accumulation rate of PD-L1 antibodies limit the incorporation of conventional radionuclides with short half-lives (^{18}F or ^{68}Ga). The pretargeting strategy can overcome the problems of slow pharmacokinetics of radiolabeled antibodies *in vivo* and the difficulty of using short half-

https://doi.org/10.1021/acsomega.4c01063
ACS Omega 2024, 9, 36969−36981

life radionuclides for PET imaging. The click reaction between Tz and TCO is one of the fastest biorthogonal click conjugation methods, making it highly suitable for pretargeted nuclear imaging strategies. A previous study used atezolizumab-TCO/[^{99m}Tc]HYNIC-PEG$_{11}$-Tz for a pretargeted single photon emission computed tomography (SPECT) imaging study, which successfully detected PD-L1 expression in vivo.[46] However, in the realm of radionuclide imaging, PET outshines SPECT with its heightened spatial resolution and sensitivity. These attributes enable more accurate dynamic imaging and dose quantification. Therefore, it is important to develop a pretargeted imaging strategy based on PET imaging for the detection of PD-L1 expression.

In this study, we investigated the pretargeted PET imaging of A549-PDL1 xenografts utilizing the Diels−Alder click chemistry reaction between a ^{18}F-labeled methyl tetrazine and a TCO-functionalized anti-PDL1 antibody.

^{18}F is the most frequently employed positron-emitting isotope in clinical practice, offering advantages including easy accessibility, high image quality, and a clinically suitable half-life ($t_{1/2}$ = 109.8 min). Attachment of a NOTA functional group to this linker provided a chelator that could be effectively utilized for both ^{18}F aluminum and ^{68}Ga. In our initial study, we linked ^{18}F directly to methyl tetrazine and found that [^{18}F]Tz accumulated in large amounts in liver and was cleared slowly in vivo, which was not conducive to late pretargeted imaging. In a previous study, the inclusion of PEG linkers was found to expedite the clearance of radiopharmaceuticals and reduce uptake in tissues that are not the target;[47] therefore we designed two additional compounds with different numbers of PEG groups (6, 12) conjugated to the NOTA functional group. Subsequently, three ^{18}F-labeled methyl tetrazine radioligands were successfully synthesized by using the aluminum fluoride labeling method.

Atezolizumab and durvalumab are the most commonly used targeted PD-L1 antibodies in cancer immunotherapy with similar mechanisms of action but varying levels of efficacy. Labeling the two antibodies with radioactive isotopes allows for analysis and monitoring of their in vitro binding and in vivo pharmacokinetic properties, which can help further elucidate the pharmacological differences between the two antibodies. In vitro radiolabeling between [^{18}F]Tz and atezolizumab/durvalumab-TCO was completed within 10 min and resulted in successful radiolabeling of atezolizumab/durvalumab-TCO with high radiochemical yields, demonstrating the suitability of the method for radiolabeling of antibodies with ^{18}F in mild reaction conditions. The specificity of PD-L1 pretargeting was confirmed based on the significantly higher uptake in durvalumab/atezolizumab-TCO pretreated A549-PDL1 cells compared to untreated cells, while this uptake could be blocked by using a high amount of the PD-L1 antibodies and unlabeled tetrazine. Interestingly, the experimental results show significant differences in the uptake and internalization of A549-PDL1 cells between [^{18}F]Tz-TCO-durvalumab and [^{18}F]Tz-TCO-atezolizumab. These differences may stem from the inherent characteristics of the two antibodies, which warrant further investigation.

The elimination rate of tetrazine compound [^{18}F]Tz was slower when used alone and was mainly cleared by the hepatobiliary system. A large amount of residual activity was found in liver at 1 h p.i. in mice, which may interfere with the subsequent image quality. Based on the structure of NOTA-Tz, 6 and 12 PEG groups were introduced, significantly increasing the hydrophilicity of the tetrazine derivative, and the hepatic and biliary clearance was transformed into renal clearance. This improvement successfully reduced the liver uptake of the tetrazine derivative by 9.5-fold and 14-fold, respectively. However, ex vivo biodistribution studies of [^{18}F]PEG$_6$-Tz revealed that there was still a high radioactive uptake in the gallbladder at 1 h p.i. in mice. Compared to [^{18}F]Tz and [^{18}F]PEG$_6$-Tz, [^{18}F]PEG$_{12}$-Tz demonstrates a faster in vivo clearance rate and lower nontarget uptake. As a result, [^{18}F]PEG$_{12}$-Tz emerges as the most promising tetrazine radioactive ligand for pretargeted imaging studies.

The pretargeted biodistribution and imaging experiment of durvalumab/atezolizumab-TCO in A549-PDL1 xenografts demonstrated significant differences in the pharmacokinetics of the two antibodies within the body. Tumor uptake of durvalumab-TCO peaked at 24 h and gradually decreased thereafter. In contrast, the tumor uptake of atezolizumab-TCO/[^{18}F]PEG$_{12}$-Tz initially increases and peaks at 48 h, after which it gradually declines. The experimental results indicate that atezolizumab-TCO is more suitable for pretargeted PET imaging, and the optimal imaging time is 48 h after atezolizumab-TCO administration. The tumor/muscle ratio based on the region of interest (ROI) values outlined in the PET image data can reach up to 21.6, a contrast that was high enough for PD-L1 imaging. The tumor/muscle ratio of 21.6 from PET image data was higher than the tumor/muscle ratio of 5.33 from biodistribution data, which may be due to differences in the algorithms of the image software and the location of the outlined target areas.

The experimental results of A549-PDL1 and A549 xenografts also indicate that the pretargeting atezolizumab-TCO/[^{18}F]PEG$_{12}$-Tz can specifically identify the expression status of PD-L1 in the tumor. Moreover, the accumulation of pretargeting atezolizumab-TCO/[^{18}F]PEG$_{12}$-Tz in A549-PDL1 tumors could be blocked by co-injection of additional unmodified anti-PD-L1 antibody or unlabeled tetrazine, which indicated that it was a PD-L1-specific uptake.

The relatively short biological half-life of ^{18}F restricted us to tracking in vitro labeled atezolizumab for only a few hours. Therefore, we compared the PET imaging data of the directly labeled antibody [^{18}F]Tz-TCO-atezolizumab probe with the pretargeted imaging. The data showed that the PET image contrast of pretargeted atezolizumab-TCO/[^{18}F]PEG$_{12}$-Tz was significantly superior to the imaging results 8 h after direct injection of [^{18}F]Tz-TCO-atezolizumab. In addition, the dosimetric calculations revealed significantly lower absorbed doses for the pretargeted approach, which demonstrates the dosimetric advantage of the pretargeted approach compared to that of the conventional direct antibody radiolabeling strategy even with the same radionuclide, fluorine-18. Furthermore, the internal radiation doses of this pretargeted approach in humans are also considered safe for clinical application.

CONCLUSIONS

In this study, three ^{18}F-labeled methyl tetrazines ([^{18}F]Tz, [^{18}F]PEG$_6$-Tz, and [^{18}F]PEG$_{12}$-Tz) were designed, synthesized, and subjected to biological evaluation. Among these derivatives, [^{18}F]PEG$_{12}$-Tz with 12 PEGs displayed optimal in vivo pharmacokinetics and could undergo rapid Diels−Alder reaction with both TCO-modified PD-L1 antibodies (durvalumab/atezolizumab-TCO) in vitro and in vivo. Biodistribution and PET imaging experiments indicated that the pretargeted strategy (atezolizumab-TCO/[^{18}F]PEG$_{12}$-Tz)

https://doi.org/10.1021/acsomega.4c01063
ACS Omega 2024, 9, 36969−36981

could evaluate the PD-L1 expression level and was highly effective at delineating the A549-PDL1 tumor from normal tissue, producing PET images with relatively high contrast. The pretargeted imaging strategy of this study can serve as a powerful tool to assess PD-L1 for further clinical translational applications.

■ ASSOCIATED CONTENT

Supporting Information

The Supporting Information is available free of charge at https://pubs.acs.org/doi/10.1021/acsomega.4c01063.

Characterization of NOTA-Tz, NOTA-PEG_6-Tz, NOTA-PEG_{12}-Tz, and durvalumab/atezolizumab-TCO, ligation of durvalumab-TCO with [^{18}F]Tz, stability of [^{18}F]PEG_{12}-Tz and [^{18}F]Tz-TCO-atezolizumab, Western blot, immunohistochemical staining, saturation binding, PET imaging, and estimated human dosimetry (PDF)

■ AUTHOR INFORMATION

Corresponding Authors

Ying Liang − *Department of Nuclear Medicine, National Cancer Center/National Clinical Research Center for Cancer/Cancer Hospital & Shenzhen Hospital, Chinese Academy of Medical Sciences and Peking Union Medical College, Shenzhen 518116, China*; Email: liangy_2000@sina.com

Qi Liu − *International Cancer Center, Shenzhen University School of Medicine, Shenzhen University, Shenzhen 518060, China*; orcid.org/0000-0002-3285-7864; Email: liu_qi@szu.edu.cn

Authors

Yong Huang − *Department of Nuclear Medicine, National Cancer Center/National Clinical Research Center for Cancer/Cancer Hospital & Shenzhen Hospital, Chinese Academy of Medical Sciences and Peking Union Medical College, Shenzhen 518116, China*; orcid.org/0009-0005-7282-3166

Zhongjing Li − *Department of Nuclear Medicine, National Cancer Center/National Clinical Research Center for Cancer/Cancer Hospital & Shenzhen Hospital, Chinese Academy of Medical Sciences and Peking Union Medical College, Shenzhen 518116, China*

Chengze Li − *Department of Nuclear Medicine, National Cancer Center/National Clinical Research Center for Cancer/Cancer Hospital & Shenzhen Hospital, Chinese Academy of Medical Sciences and Peking Union Medical College, Shenzhen 518116, China*

Zihan Zang − *Shenzhen Middle School, Shenzhen 518024, China*

Qiong Wang − *Department of Nuclear Medicine, National Cancer Center/National Clinical Research Center for Cancer/Cancer Hospital & Shenzhen Hospital, Chinese Academy of Medical Sciences and Peking Union Medical College, Shenzhen 518116, China*

Size Huang − *Department of Nuclear Medicine, National Cancer Center/National Clinical Research Center for Cancer/Cancer Hospital & Shenzhen Hospital, Chinese Academy of Medical Sciences and Peking Union Medical College, Shenzhen 518116, China*

Complete contact information is available at: https://pubs.acs.org/10.1021/acsomega.4c01063

Author Contributions

This research study was designed by YH and QL. Synthesis, radiosynthesis, and analysis of the chemical data were performed by CL and YH. In vitro and in vivo experiments were performed by YH, ZL, CL, ZZ, QW, and SH and supervised by YH, QL, and YL. Data analysis was performed by ZL and YH. The first draft of the manuscript was written by YH, and all authors commented on previous versions of the manuscript. YH and YL made substantial contributions to the interpretation of the data and revised the manuscript critically for important intellectual content.

Funding

This research was funded by the National Natural Science Foundation of China (82102115 and 82373212), the National Cancer Center, the National Clinical Research Center for Cancer, the Cancer Hospital and Shenzhen Hospital, the Chinese Academy of Medical Sciences and Peking Union Medical College, Shenzhen (E010321007), the Shenzhen High-level Hospital Construction Fund, the Shenzhen Science and Technology Program of China (JCYJ20220818101804009), and the Shenzhen Clinical Research Center for Cancer (No. (2021) 287).

Notes

The authors declare no competing financial interest.

■ ACKNOWLEDGMENTS

We thank Prof. Yang Zhi from the Peking University Cancer Hospital for providing us with A549-PDL1 cells.

■ REFERENCES

(1) Yi, M.; Niu, M.; Xu, L.; Luo, S.; Wu, K. Regulation of PD-L1 expression in the tumor microenvironment. *Journal of hematology oncology* **2021**, *14* (1), 10.

(2) Jiang, X.; Wang, J.; Deng, X.; Xiong, F.; Ge, J.; Xiang, B.; Wu, X.; Ma, J.; Zhou, M.; Li, X.; et al. Role of the tumor microenvironment in PD-L1/PD-1-mediated tumor immune escape. *Molecular cancer* **2019**, *18* (1), 10.

(3) Shklovskaya, E.; Rizos, H. Spatial and temporal changes in PD-L1 expression in cancer: the role of genetic drivers, tumor microenvironment and resistance to therapy. *International Journal of Molecular Sciences* **2020**, *21* (19), 7139.

(4) Chen, X. J.; Yuan, S. Q.; Duan, J. L.; Chen, Y. M.; Chen, S.; Wang, Y.; Li, Y. F. The value of PD-L1 expression in predicting the efficacy of anti-PD-1 or anti-PD-L1 therapy in patients with cancer: a systematic review and meta-analysis. *Disease Markers* **2020**, *2020*, 1−14.

(5) Gandini, S.; Massi, D.; Mandalà, M. PD-L1 expression in cancer patients receiving anti PD-1/PD-L1 antibodies: A systematic review and meta-analysis. *Critical reviews in oncology/hematology* **2016**, *100*, 88−98.

(6) Xu, Y.; Wan, B.; Chen, X.; Zhan, P.; Zhao, Y.; Zhang, T.; Liu, H.; Afzal, M. Z.; Dermime, S.; Hochwald, S. N.; et al. The association of PD-L1 expression with the efficacy of anti-PD-1/PD-L1 immunotherapy and survival of non-small cell lung cancer patients: a meta-analysis of randomized controlled trials. *Translational Lung Cancer Research* **2019**, *8* (4), 413.

(7) Chen, L.; Han, X. Anti-PD-1/PD-L1 therapy of human cancer: past, present, and future. *J. Clin. Invest.* **2015**, *125* (9), 3384−3391.

(8) Mathieu, L.; Shah, S.; Pai-Scherf, L.; Larkins, E.; Vallejo, J.; Li, X.; Rodriguez, L.; Mishra-Kalyani, P.; Goldberg, K. B.; Kluetz, P. G.; Theoret, M. R.; Beaver, J. A.; Pazdur, R.; Singh, H. FDA Approval Summary: Atezolizumab and Durvalumab in Combination with

Platinum-Based Chemotherapy in Extensive Stage Small Cell Lung Cancer. *Oncologist* **2021**, *26* (5), 433−438.
(9) Chen, J.; Wang, J.; Xu, H. Comparison of atezolizumab, durvalumab, pembrolizumab, and nivolumab as first-line treatment in patients with extensive-stage small cell lung cancer: A systematic review and network meta-analysis. *Medicine* **2021**, *100* (15), e25180.
(10) Ionova, Y.; Vuong, W.; Sandoval, O.; Fong, J.; Vu, V.; Zhong, L.; Wilson, L. Cost-effectiveness analysis of atezolizumab versus durvalumab as first-line treatment of extensive-stage small-cell lung cancer in the USA. *Clinical Drug Investigation* **2022**, *42* (6), 491−500.
(11) Muehllehner, G.; Karp, J. S. Positron emission tomography. *Physics in Medicine & Biology* **2006**, *51* (13), R117.
(12) Yasuda, S.; Ide, M.; Fujii, H.; Nakahara, T.; Mochizuki, Y.; Takahashi, W.; Shohtsu, A. Application of positron emission tomography imaging to cancer screening. *British Journal of cancer* **2000**, *83* (12), 1607−1611.
(13) Walker, S. M.; Lim, I.; Lindenberg, L.; Mena, E.; Choyke, P. L.; Turkbey, B. Positron emission tomography (PET) radiotracers for prostate cancer imaging. *Abdominal Radiology* **2020**, *45*, 2165−2175.
(14) Smit, J.; Borm, F. J.; Niemeijer, A. L. N.; Huisman, M. C.; Hoekstra, O. S.; Boellaard, R.; Oprea-Lager, D. E.; Vugts, D. J.; van Dongen, G. A.; Thunnissen, E.; et al. PD-L1 PET/CT Imaging with Radiolabeled Durvalumab in Patients with Advanced-Stage Non-Small Cell Lung Cancer. *J. Nucl. Med.* **2021**, *63* (5), 686−693.
(15) Lesniak, W. G.; Chatterjee, S.; Gabrielson, M.; Lisok, A.; Wharram, B.; Pomper, M. G.; Nimmagadda, S. PD-L1 detection in tumors using [^{64}Cu] atezolizumab with PET. *Bioconjugate Chem.* **2016**, *27* (9), 2103−2110.
(16) Jagoda, E. M.; Vasalatiy, O.; Basuli, F.; Opina, A. C. L.; Williams, M. R.; Wong, K.; Lane, K. C.; Adler, S.; Ton, A. T.; Szajek, L. P.; et al. Immuno-PET imaging of the programmed cell death-1 ligand (PD-L1) using a zirconium-89 labeled therapeutic antibody, avelumab. *Molecular imaging* **2019**, *18*, 153601211982998.
(17) Christensen, C.; Kristensen, L. K.; Alfsen, M. Z.; Nielsen, C. H.; Kjaer, A. Quantitative PET imaging of PD-L1 expression in xenograft and syngeneic tumour models using a site-specifically labelled PD-L1 antibody. *European Journal of Nuclear Medicine and Molecular Imaging* **2020**, *47*, 1302−1313.
(18) Liu, Q.; Jiang, L.; Li, K.; Li, H.; Lv, G.; Lin, J.; Qiu, L. Immuno-PET imaging of ^{68}Ga-labeled nanobody Nb109 for dynamic monitoring the PD-L1 expression in cancers. *Cancer Immunology, Immunotherapy* **2021**, *70*, 1721−1733.
(19) Chatterjee, S.; Lesniak, W. G.; Miller, M. S.; Lisok, A.; Sikorska, E.; Wharram, B.; Kumar, D.; Gabrielson, M.; Pomper, M. G.; Gabelli, S. B.; Nimmagadda, S. Rapid PD-L1 detection in tumors with PET using a highly specific peptide. *Biochem Biophys Rapid Commun* **2017**, *483* (1), 258−263.
(20) Lesniak, W. G.; Mease, R. C.; Chatterjee, S.; Kumar, D.; Lisok, A.; Wharram, B.; Kalagadda, V. R.; Emens, L. A.; Pomper, M. G.; Nimmagadda, S. Development of [^{18}F] FPy-WL12 as a PD-L1 specific PET imaging peptide. *Molecular imaging* **2019**, *18*, 153601211985218.
(21) Zhou, X.; Jiang, J.; Yang, X.; Liu, T.; Ding, J.; Nimmagadda, S.; Pomper, M. G.; Zhu, H.; Zhao, J.; Yang, Z.; Li, N. First-in-Humans Evaluation of a PD-L1-Binding Peptide PET Radiotracer in Non-Small Cell Lung Cancer Patients. *J. Nucl. Med.* **2022**, *63* (4), 536−542.
(22) Xu, L.; Zhang, L.; Liang, B.; Zhu, S.; Lv, G.; Qiu, L.; Lin, J. Design, Synthesis, and Biological Evaluation of a Small-Molecule PET Agent for Imaging PD-L1 Expression. *Pharmaceuticals* **2023**, *16* (2), 213.
(23) Krutzek, F.; Donat, C. K.; Ullrich, M.; Stadlbauer, S. Design, Synthesis, and Biological Evaluation of Small-Molecule-Based Radioligands with Improved Pharmacokinetic Properties for Imaging of Programmed Death Ligand 1. *J. Med. Chem.* **2023**, *66* (23), 15894−15915.
(24) Krutzek, F.; Donat, C. K.; Ullrich, M.; Zarschler, K.; Ludik, M. C.; Feldmann, A.; Loureiro, L. R.; Kopka, K.; Stadlbauer, S. Design and Biological Evaluation of Small-Molecule PET-Tracers for Imaging of Programmed Death Ligand 1. *Cancers* **2023**, *15* (9), 2638.
(25) Huang, Y.; Li, C.; Li, Z.; Wang, Q.; Huang, S.; Liu, Q.; Liang, Y. Development and Preclinical Evaluation of [^{68}Ga] BMSH as a New Potent Positron Emission Tomography Tracer for Imaging Programmed Death-Ligand 1 Expression. *Pharmaceuticals* **2023**, *16* (10), 1487.
(26) Huisman, M. C.; Niemeijer, A. L. N.; Windhorst, A. D.; Schuit, R. C.; Leung, D.; Hayes, W.; Poot, A.; Bahce, I.; Radonic, T.; Oprea-Lager, D. E.; et al. Quantification of PD-L1 expression with ^{18}F-BMS-986192 PET/CT in patients with advanced-stage non-small cell lung cancer. *J. Nucl. Med.* **2020**, *61* (10), 1455−1460.
(27) Zhou, M.; Wang, X.; Chen, B.; Xiang, S.; Rao, W.; Zhang, Z.; Liu, H.; Fang, J.; Yin, X.; Deng, P.; et al. Preclinical and first-in-human evaluation of ^{18}F-labeled D-peptide antagonist for PD-L1 status imaging with PET. *European Journal of Nuclear Medicine and Molecular Imaging* **2022**, *49* (13), 4312−4324.
(28) Zhou, Y.; Baidoo, K. E.; Brechbiel, M. W. Mapping biological behaviors by application of longer-lived positron emitting radionuclides. *Advanced drug delivery reviews* **2013**, *65* (8), 1098−1111.
(29) Vivier, D.; Sharma, S. K.; Zeglis, B. M. Understanding the in vivo fate of radioimmunoconjugates for nuclear imaging. *Journal of Labelled Compounds and Radiopharmaceuticals* **2018**, *61* (9), 672−692.
(30) Price, E. W.; Orvig, C. The Chemistry of Inorganic Nuclides (^{86}Y, ^{68}Ga, ^{64}Cu, ^{89}Zr, ^{124}I). *Chemistry of Molecular Imaging* **2014**, 105−135.
(31) Boros, E.; Packard, A. B. Radioactive transition metals for imaging and therapy. *Chem. Rev.* **2019**, *119* (2), 870−901.
(32) Shokeen, M.; Anderson, C. J. Molecular Imaging of Cancer with Copper-64 Radiopharmaceuticals and Positron Emission Tomography (PET). *Acc. Chem. Res.* **2009**, *42* (7), 832−841.
(33) Nayak, T. K.; Brechbiel, M. W. Radioimmunoimaging with longer-lived positron-emitting radionuclides: potentials and challenges. *Bioconjugate Chem.* **2009**, *20* (5), 825−841.
(34) Wu, H.; Devaraj, N. K. Inverse electron-demand Diels-Alder bioorthogonal reactions. *Cycloadditions in Bioorthogonal Chemistry* **2016**, 109−130.
(35) Qiu, L.; Mao, W.; Yin, H.; Tan, H.; Cheng, D.; Shi, H. Pretargeted Nuclear Imaging and Radioimmunotherapy Based on the Inverse Electron-Demand Diels-Alder Reaction and Key Factors in the Pretargeted Synthetic Design. *Contrast Media & Molecular Imaging* **2019**, *2019*, 1−12.
(36) Johann, K.; Svatunek, D.; Seidl, C.; Rizzelli, S.; Bauer, T. A.; Braun, L.; Koynov, K.; Mikula, H.; Barz, M. Tetrazine-andtrans-cyclooctene-functionalised polypept(o)ides for fast bioorthogonal tetrazine ligation. *Polym. Chem.* **2020**, *11* (27), 4396−4407.
(37) Zhang, R.; Gao, J.; Zhao, G.; Zhou, L.; Kong, F.; Jiang, T.; Jiang, H. Tetrazine bioorthogonal chemistry makes nanotechnology a powerful toolbox for biological applications. *Nanoscale* **2023**, *15* (2), 461−469.
(38) Yi, W.; Xiao, P.; Liu, X.; Zhao, Z.; Sun, X.; Wang, J.; Zhou, L.; Wang, G.; Cao, H.; Wang, D.; Li, Y. Recent advances in developing active targeting and multi-functional drug delivery systems via bioorthogonal chemistry. *Signal Transduction and Targeted Therapy* **2022**, *7* (1), 386.
(39) Nguyen, S. S.; Prescher, J. A. Developing bioorthogonal probes to span a spectrum of reactivities. *Nature Reviews Chemistry* **2020**, *4* (9), 476−489.
(40) Meyer, J. P.; Houghton, J. L.; Kozlowski, P.; Abdel-Atti, D.; Reiner, T.; Pillarsetty, N. V. K.; Scholz, W. W.; Zeglis, B. M.; Lewis, J. S. ^{18}F-Based Pretargeted PET Imaging Based on Bioorthogonal Diels-Alder Click Chemistry. *Bioconjugate Chem.* **2016**, *27* (2), 298−301.
(41) Liu, G.; Wold, E. A.; Zhou, J. Applications of Bioorthogonal Chemistry in Tumor-Targeted Drug Discovery. *Curr. Top Med. Chem.* **2019**, *19* (11), 892−897.
(42) Zeglis, B. M.; Mohindra, P.; Weissmann, G. I.; Divilov, V.; Hilderbrand, S. A.; Weissleder, R.; Lewis, J. S. Modular strategy for the construction of radiometalated antibodies for positron emission tomography based on inverse electron demand diels-alder click chemistry. *Bioconjugate Chem.* **2011**, *22* (10), 2048−2059.

https://doi.org/10.1021/acsomega.4c01063
ACS Omega 2024, 9, 36969−36981

(43) Zeglis, B. M.; Sevak, K. K.; Reiner, T.; Mohindra, P.; Carlin, S. D.; Zanzonico, P.; Weissleder, R.; Lewis, J. S. A pretargeted PET imaging strategy based on bioorthogonal Diels-Alder click chemistry. *J. Nucl. Med.* **2013**, *54* (8), 1389−1396.
(44) St. Amant, A. H.; Huang, F.; Lin, J.; Lemen, D.; Chakiath, C.; Mao, S.; Fazenbaker, C.; Zhong, H.; Harper, J.; Xu, W.; et al. A reactive antibody platform for one-step production of antibody-drug conjugates through a Diels-Alder reaction with maleimide. *Bioconjugate Chem.* **2019**, *30* (9), 2340−2348.
(45) Sarrett, S. M.; Keinänen, O.; Dayts, E. J.; Dewaele-Le Roi, G.; Rodriguez, C.; Carnazza, K. E.; Zeglis, B. M. Inverse electron demand Diels-Alder click chemistry for pretargeted PET imaging and radioimmunotherapy. *Nature protocols* **2021**, *16* (7), 3348−3381.
(46) Qiu, L.; Tan, H.; Lin, Q.; Si, Z.; Mao, W.; Wang, T.; Fu, Z.; Cheng, D.; Shi, H. A Pretargeted Imaging Strategy for Immune Checkpoint Ligand PD-L1 Expression in Tumor Based on Bioorthogonal Diels-Alder Click Chemistry. *Mol. Imaging Biol.* **2020**, *22*, 842−853.
(47) Meyer, J. P.; Kozlowski, P.; Jackson, J.; Cunanan, K. M.; Adumeau, P.; Dilling, T. R.; Zeglis, B. M.; Lewis, J. S. Exploring Structural Parameters for Pretargeting Radioligand Optimization. *J. Med. Chem.* **2017**, *60* (19), 8201−8217.

https://doi.org/10.1021/acsomega.4c01063
ACS Omega 2024, 9, 36969−36981